

A brief review on cosmological analysis of galaxy surveys with multiple tracers

Yuting Wang¹ and Gong-Bo Zhao^{1,2}

¹ National Astronomical Observatories, Chinese Academy of Sciences, Beijing 100101, China; ytwang@nao.cas.cn, gbzhao@nao.cas.cn

² University of Chinese Academy of Sciences, Beijing 100049, China

Received 2020 September 15; accepted 2020 September 23

Abstract Galaxy redshift surveys are one of the key probes in modern cosmology. In the data analysis of galaxy surveys, the precision of the statistical measurement is primarily limited by the cosmic variance on large scales. Fortunately, this limitation can in principle be mitigated by observing multiple types of biased tracers. In this brief review, we present the idea of the multi-tracer method, outline key steps in the data analysis and show several worked examples based on the GAMA, BOSS and eBOSS galaxy surveys. This work is a part of a special issue dedicated to the 20th anniversary of RAA (2001–2020), which is prefaced in Wang & Ip (2020).

Key words: cosmology: large scale structure — dark energy — baryon acoustic oscillations — redshift space distortions

1 INTRODUCTION

Mapping the Universe with massive galaxy surveys provides critical cosmological information, which is key to reveal the physics governing the evolution of the Universe. In particular, galaxy surveys play a crucial role for understanding the origin of the cosmic acceleration discovered in the late 1990s (Riess et al. 1998; Perlmutter et al. 1999), which may be due to the existence of Dark Energy (see Huterer & Shafer 2018 for a recent review), an energy component with a negative pressure, or to the extension of General Relativity (GR), as reviewed in Koyama (2016).

Cosmological information in galaxy surveys is primarily encoded in the baryon acoustic oscillations (BAO) and the redshift space distortions (RSD), which are specific clustering patterns of biased tracers (Percival et al. 2001; Peacock et al. 2001; Eisenstein et al. 2005; Cole et al. 2005; Percival et al. 2007; Beutler et al. 2011; Blake et al. 2011; Anderson et al. 2012; Padmanabhan et al. 2012; Ross et al. 2015; Alam et al. 2017). Being complementary to other probes including supernovae (SNIa) (Riess et al. 1998; Perlmutter et al. 1999; Riess et al. 2007; Sullivan et al. 2011; Suzuki et al. 2012; Betoule et al. 2014; Scolnic et al. 2018; D’Andrea et al. 2018) and cosmic microwave background (CMB) (Bennett et al. 2003; Hinshaw et al. 2013; Planck Collaboration et al. 2018), the BAO, as a

standard ruler, map the expansion history of the Universe, and thus are essential to constraining dark energy, while the RSD, caused by peculiar motions of galaxies, are a natural probe for the nature of gravity on cosmological scales.

Great progress on galaxy surveys has been made since last century. Starting in the 1970s, the Harvard-Smithsonian Center for Astrophysics (CfA) redshift survey brought us the first large galaxy sample, which consisted of several thousand galaxies for a clustering analysis (Huchra et al. 1983; Davis & Peebles 1983). Thanks to technical developments related to multi-object spectrographs and charge coupled device (CCD)-based photometry, larger galaxy surveys have been planned and carried out since then, including the Las Campanas Redshift Survey (Shectman et al. 1996), the Sloan Digital Sky Survey (SDSS) (York et al. 2000), 2dF Galaxy Redshift Survey (2dFGRS) (Colless et al. 2001), WiggleZ Dark Energy Survey (Blake et al. 2008), 6dF Galaxy Survey (6dFGS) (Jones et al. 2009), Galaxy And Mass Assembly (GAMA) survey (Baldry et al. 2010), etc.

Based on the 2.5-meter Sloan Telescope (Gunn et al. 2006) installed at Apache Point Observatory, the SDSS project has been one of the most powerful and successful galaxy surveys in the world during the last two decades, with the timeline for the past four generations being: SDSS-I and II (Abazajian et al. 2009) (1998–2008), SDSS-III/Baryon Oscillation Spectroscopic Survey (Eisenstein

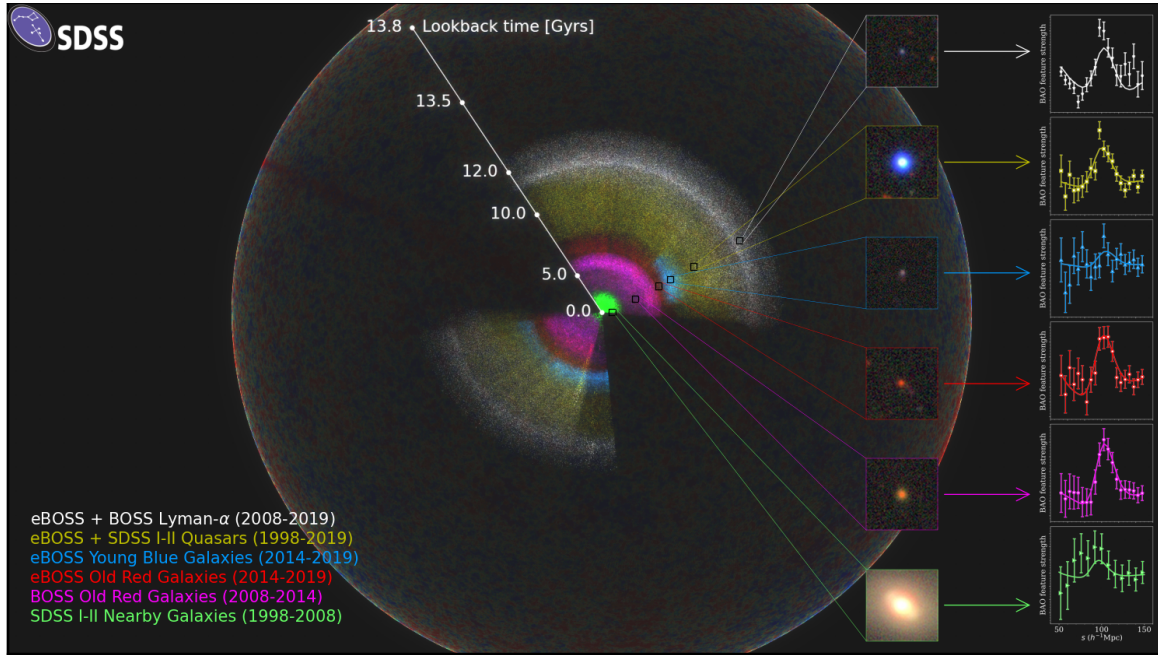


Fig. 1 Mapping the Universe in three dimensions with SDSS (1998–2020) using different types of tracers including galaxies, quasars and Lyman- α forest, as illustrated using different colors. The outermost is the last scattering surface of the CMB. The six panels on the right are the BAO-peak measurements utilizing different samples, as labeled in the legend in the lower-left corner. Image credit: Anand Raichoor (EPFL), Ashley Ross (Ohio State University) and the SDSS Collaboration. This image is a part of the eBOSS DR16 press release, which is available at <https://www.sdss.org/press-releases/no-need-to-mind-the-gap/>.

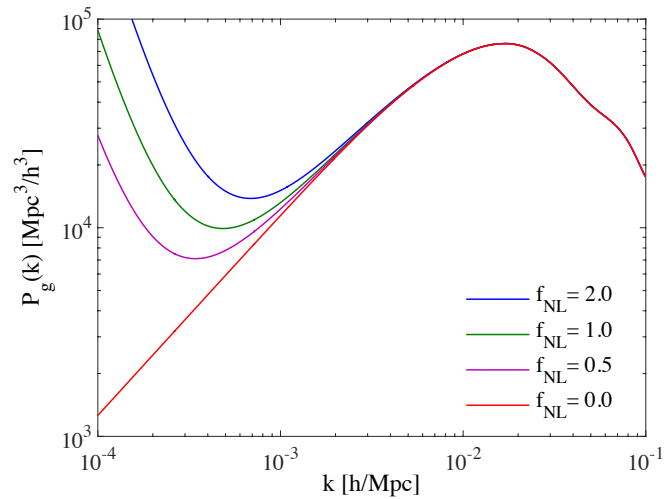


Fig. 2 The galaxy power spectrum for different values of f_{NL} , as displayed in the legend.

et al. 2011) (BOSS; 2008–2014), and SDSS-IV/extended Baryon Oscillation Spectroscopic Survey (Dawson et al. 2016) (eBOSS; 2014–2020). SDSS has created by far the largest map of the Universe by observing various kinds of tracers, as depicted in Figure 1.

As key quantities for cosmological implications, BAO and RSD are measured from almost all available wide-field galaxy surveys. The statistical uncertainties of BAO and RSD parameters are inherited from the uncertainty in the

two-point statistics of galaxy clustering, which consist of two components: the shot noise and the cosmic variance. While the former can be suppressed by increasing the number density of tracers in the observation, the latter cannot be reduced statistically, as long as only one tracer is observed, because of the limited number of pairs on large scales. However, if at least two tracers with an overlapping cosmic volume are observed, the cosmic variance can be reduced to some extent, depending on the level of

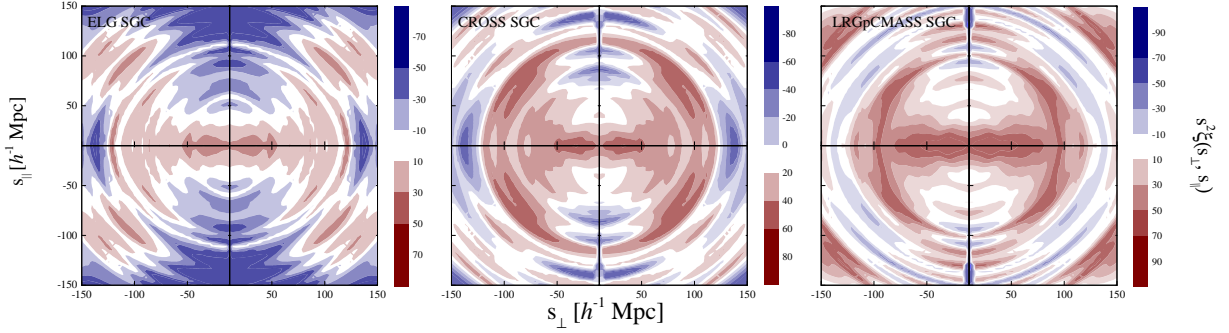


Fig. 3 The 2D auto- and cross-correlation functions $\xi(s, \mu)$ generated considering the monopole, quadrupole and hexadecapole measurements applying the estimator in Eq. (11), where $s^2 = s_{\parallel}^2 + s_{\perp}^2$, from the samples of eBOSS DR16 ELG (*left*), LRG (*right*), and their cross-correlation (*middle*) in the South Galactic Cap. This figure is adopted from Wang et al. (2020).

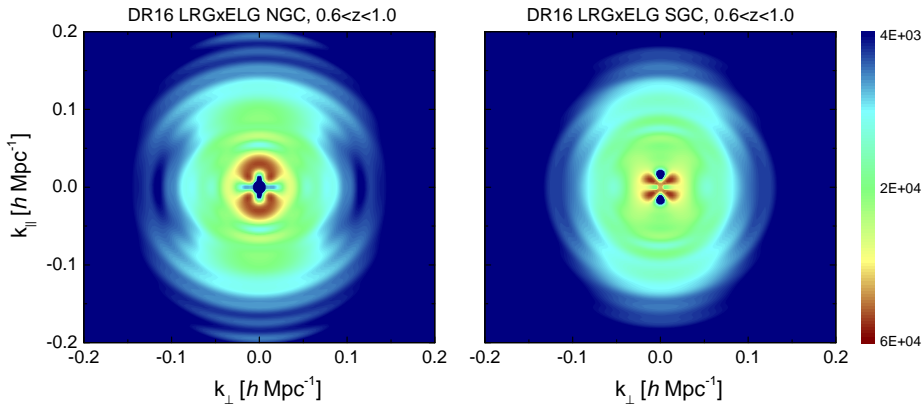


Fig. 4 The cross power spectrum between the eBOSS DR16 LRGs and ELGs in the Northern (*left*) and Southern Galactic Cap (*right*) measured using the estimator Eq. (15). This figure is adopted from Zhao et al. (2020).

shot noise (Seljak 2009; McDonald & Seljak 2009). This ‘multi-tracer method’ works if at least two differently biased tracers of the same underlying dark matter field are available. By comparing the galaxy clustering of these tracers, one is able to determine a ratio between the ‘effective biases’, which may include the RSD parameter β , and the primordial non-Gaussianity parameter f_{NL} , to an infinite accuracy in the zero noise limit, as detailed in Section 2. The validity of this method has been extensively studied (White et al. 2009; Gil-Marín et al. 2010; Bernstein & Cai 2011; Hamaus et al. 2011; Abramo 2012; Cai & Bernstein 2012; Abramo & Leonard 2013; Ferramacho et al. 2014; Yamauchi et al. 2014; Abramo et al. 2016; Zhao et al. 2016; Alarcon et al. 2018; Abramo & Amendola 2019; Boschetti et al. 2020; Viljoen et al. 2020).

Applying this method to actual galaxy surveys requires finding at least two differently biased tracers covering the same patch of sky and redshift range. This is challenging for most existing surveys, which are designed and optimized for a single tracer within a given footprint

and redshift range. One possibility to create such ‘multi-tracer’ samples from a single-tracer survey is to split the sample into subsamples by luminosity or color (Blake et al. 2013; Ross et al. 2014), but this may be subject to a limited relative galaxy bias, as samples in a single-tracer survey usually do not differ much in the galaxy bias. Alternatively, one can combine tracers observed by different surveys (Marín et al. 2016; Beutler et al. 2016). However, this approach could be limited by the small overlapping area, as most galaxy surveys are designed to be complementary to each other, in terms of sky coverage and/or redshift range.

Fortunately, the SDSS-IV/eBOSS survey has created a great opportunity for a proper multi-tracer analysis, as it is the first galaxy survey to observe multiple tracers with a large overlap in the cosmic volume. Targeting both the luminous red galaxies (LRGs, labeled as ‘Old Red Galaxies’ in Fig. 1 at $0.6 < z < 1.0$), and emission line galaxies (ELGs, ‘Young Blue Galaxies’ in Fig. 1 at $0.6 < z < 1.1$), eBOSS offers observations of the clustering of these two tracers in a large overlapping area

(over 700 deg²) in the same redshift range (Dawson et al. 2016). A multi-tracer analysis on the final eBOSS sample, which is tagged as the Data Release (DR)16 data sample, was performed in both the configuration space (Wang et al. 2020) and Fourier space (Zhao et al. 2020).

This article serves as a brief review of the multi-tracer analysis of galaxy surveys, including the methodology (Sect. 2), key steps in the analysis (Sect. 3) and recent cosmological implications (Sect. 4). Section 5 is devoted to summary and a future outlook.

2 THE MULTI-TRACER METHOD

We start with a matter over-density field, namely, $\delta_m \equiv (\rho - \bar{\rho})/\bar{\rho}$ with $\bar{\rho}$ being the mean density. The observed galaxy traces the matter field up to an effective bias factor b_g , relating the over-density of the observed galaxy δ_g to matter δ_m on linear scales, *i.e.*, $\delta_g = b_g \delta_m$. The measured 2-point statistics of δ_g , *e.g.*, the power spectrum, $P_g \equiv \langle \delta_g \delta_g \rangle = b_g^2 P_m$, is subject to the cosmic variance and the shot noise, which dominate the error budget on large and small scales, respectively.

If two tracers for the same underlying matter density field are available, then the ratio between δ_{g2} and δ_{g1} is,

$$\frac{\delta_{g2}}{\delta_{g1}} = \frac{b_{g2} \delta_m + \epsilon_{g2}}{b_{g1} \delta_m + \epsilon_{g1}}, \quad (1)$$

2.1 Determining the RSD Parameter with Multi-tracer Surveys

In redshift surveys, the radial distance of a galaxy is inferred from the observed redshift, which is determined by the underlying Hubble flow and the peculiar velocity of a galaxy along the line of sight. Hence, the observed galaxy position in redshift space x^s is,

$$x^s = x + \frac{\mathbf{v} \cdot \hat{\mathbf{r}}}{H}, \quad (4)$$

where x is the galaxy position in real-space, \mathbf{v} the peculiar velocity of a galaxy and $\hat{\mathbf{r}}$ the unit vector along the line of sight. Statistically there is an enhancement of galaxy clustering along the line of sight on large scales due to this peculiar motion, dubbed the RSD. According to linear perturbation theory, the relation between velocity and matter over-density reads,

$$-ik^2 \mathbf{v} = fH \delta_m \mathbf{k}, \quad (5)$$

where $f = d \ln \delta_m / d \ln a$ is the growth rate of structure and \mathbf{k} is the wave-number in Fourier space. Then the redshift-space galaxy density fluctuation on linear scales is given by (Kaiser 1987),

$$\delta_g = (b_g + f\mu^2) \delta_m + \epsilon_g, \quad (6)$$

where μ is the cosine of the angle between \mathbf{k} and the line of sight. Now the data covariance matrix becomes,

$$C = \frac{P_{\theta\theta}}{2} \begin{bmatrix} (\beta^{-1} + \mu^2)^2 & (\beta^{-1} + \mu^2) (\alpha\beta^{-1} + \mu^2) \\ (\beta^{-1} + \mu^2) (\alpha\beta^{-1} + \mu^2) & (\alpha\beta^{-1} + \mu^2)^2 \end{bmatrix} + \frac{N}{2}, \quad (7)$$

where $\beta \equiv f/b_{g1}$, $\alpha \equiv b_{g2}/b_{g1}$, $P_{\theta\theta} \equiv 2f^2 \langle \delta_m^2 \rangle$ and $N_{ij} \equiv 2 \langle \epsilon_i \epsilon_j \rangle$. Denoting $X_{ij} = N_{ij}/b_i b_j P_m$, McDonald & Seljak (2009) demonstrate that using only the transverse and radial modes (*i.e.* the modes with $\mu = 0$ and $\mu = 1$), the

where ϵ denotes the Poisson noise. We can immediately see that in the low-noise limit, *i.e.*, $\epsilon \rightarrow 0$, the ratio becomes $\delta_{g2}/\delta_{g1} = b_{g2}/b_{g1}$, thus it is free from the cosmic variance, as δ_m is canceled out. Because the RSD parameter $\beta \equiv f/b$ and the primordial non-Gaussianity parameter f_{NL} are part of the effective bias here, the multi-tracer method can in principle improve the constraints on β (McDonald & Seljak 2009) and f_{NL} (Seljak 2009). In practice, the dependence on δ_m cannot be completely eliminated due to the shot noise, thus the gain from multiple tracers can be downgraded by various factors including the signal-to-noise ratio of each tracer, overlapping volume, relative bias, *etc.* (Gil-Marín et al. 2010).

The general data covariance matrix for a 2-tracer system is,

$$C \equiv \begin{bmatrix} \langle \delta_{g1}^2 \rangle & \langle \delta_{g1} \delta_{g2} \rangle \\ \langle \delta_{g2} \delta_{g1} \rangle & \langle \delta_{g2}^2 \rangle \end{bmatrix}, \quad (2)$$

and the Fisher matrix can be evaluated as (Tegmark et al. 1997),

$$F_{\lambda\lambda'} = \frac{1}{2} \text{Tr} [C_{,\lambda} C^{-1} C_{,\lambda'} C^{-1}], \quad (3)$$

where $C_{,\lambda} \equiv dC/d\lambda$.

In what follows, we shall apply this result to cases of RSD and primordial non-Gaussianity.

uncertainty of β is (with α and $P_{\theta\theta}$ marginalized over),

$$\frac{\sigma_\beta^2}{\beta^2} = \frac{[\alpha^2(1+\beta)^2 + (\alpha+\beta)^2] X_{11} - 2[\alpha^2(1+\beta)^2 + \alpha(1+\beta)(\alpha+\beta)] X_{12} + 2\alpha^2(1+\beta)^2 X_{22}}{\beta^2(\alpha-1)^2}, \quad (8)$$

which goes to zero if $X \rightarrow 0$, meaning that β can be measured without the cosmic variance from a multi-tracer survey.

2.2 Determining f_{NL} with Multi-tracer Surveys

The local-type of the primordial non-Gaussianity (see [Wands 2010](#) for a review) can be described by a quadratic correction to the Gaussian field ϕ , *i.e.*, $\Phi = \phi + f_{\text{NL}}(\phi^2 - \langle \phi^2 \rangle)$, in which f_{NL} describes the amplitude of the non-Gaussian correction. This leads to a scale-dependent galaxy bias, *i.e.*, $b_g \rightarrow b_g + \Delta b(k)$ with ([Dalal et al. 2008](#); [Slosar et al. 2008](#)),

$$\Delta b(k) = 3f_{\text{NL}}(b_g - p)\delta_c \frac{\Omega_m}{k^2 T(k) D(z)} \left(\frac{H_0}{c} \right)^2, \quad (9)$$

where p depends on the type of tracer, δ_c is the critical linear over-density for spherical collapse, $T(k)$ is the matter transfer function (normalized to unity on large scales) and $D(z)$ is the growth function (normalized to a in the matter-dominated era). The galaxy over-density thus receives a k -dependent correction, say, $\delta_g = [b_g + \Delta b(k, f_{\text{NL}})] \delta_m$, which alters the shape of the power spectrum on large scales, as plotted in [Figure 2](#). This enables constraining f_{NL} with galaxy surveys ([Nikoloudakis et al. 2013](#); [Ross et al. 2013](#); [Karagiannis et al. 2014](#); [Mueller et al. 2019](#)).

As f_{NL} primarily affects the large-scale modes, its constraint can be significantly tightened if the cosmic variance is reduced. For example, the ratio of $\sigma(f_{\text{NL}})$ (with other relevant parameters marginalized over) derived from a two-tracer survey to that from a single-tracer survey using only one mode is ([Seljak 2009](#)),

$$\frac{\sigma(f_{\text{NL}})_{2\text{tr}}}{\sigma(f_{\text{NL}})_{1\text{tr}}} = \sqrt{2 \left[(n_{g2} P_{g2})^{-1} + (n_{g1} P_{g1})^{-1} \right]}, \quad (10)$$

which clearly shows that the gain can be significant in the low-noise limit.

3 THE PROCEDURE FOR A MULTI-TRACER ANALYSIS

In this section, we describe the key steps in multi-tracer analysis, including the measurement of 2-point statistics, modeling and parameter estimation.

3.1 Measuring the Galaxy Clustering

Most of the information in the clustering of galaxies is carried by its two-point correlation function, $\xi(\mathbf{s})$, or equivalently, the power spectrum in Fourier space, $P(\mathbf{k})$.

3.1.1 The correlation function

The 2-point correlation function is measured by counting pairs of galaxies at a given comoving separation, \mathbf{s} , and an unbiased estimator for two tracers, named A and B , is ([Landy & Szalay 1993](#)),

$$\xi_{AB}(s, \mu) = \frac{D_A D_B - D_A R_B - D_B R_A + R_A R_B}{R_A R_B}, \quad (11)$$

where DD , DR and RR are the normalized number pairs of galaxy-galaxy, galaxy-random and random-random, respectively, within a separation whose central value is s , and the cosine between the concerning pair and the line of sight vector is μ . The commonly-used estimator for a single tracer system is a special case of [Equation \(11\)](#) with $A = B$, namely,

$$\xi(s, \mu) = \frac{DD - 2DR + RR}{RR}. \quad (12)$$

[Figure 3](#) features the 2D auto- and cross-correlation functions measured from the eBOSS DR16 LRG and ELG samples utilizing the above estimator [Equation \(11\)](#).

3.1.2 The power spectrum

In Fourier space, the estimated power spectrum with shot noise corrected is given in (FKP estimator; Feldman et al. 1994)

$$\widehat{P}(\mathbf{k}) = \langle |F(\mathbf{k})|^2 \rangle - P_{\text{shot}}, \quad (13)$$

where $F(\mathbf{k})$ is the Fourier transformation of the weighted galaxy fluctuation field, $F(\mathbf{r})$

$$F(\mathbf{r}) = \frac{w(\mathbf{r})}{I^{1/2}} [n(\mathbf{r}) - \alpha n_s(\mathbf{r})], \quad (14)$$

with $n(\mathbf{r})$ and $n_s(\mathbf{r})$ being the observed number density field for the galaxy catalog and synthetic random catalog, respectively, and I is a normalization factor. The estimator for the auto- and cross-power spectrum for tracers A and B is (Zhao et al. 2020),

$$\widehat{P}_\ell^{\text{AB}}(k) = \frac{2\ell + 1}{2I_{\text{AB}}} \int \frac{d\Omega_k}{4\pi} [F_{0,A}(\mathbf{k})F_{\ell,B}(-\mathbf{k}) + F_{0,B}(\mathbf{k})F_{\ell,A}(-\mathbf{k})], \quad (15)$$

with

$$F_\ell(\mathbf{k}) \equiv \int d\mathbf{r} F(\mathbf{r}) e^{i\mathbf{k}\cdot\mathbf{r}} \mathcal{L}_\ell(\hat{\mathbf{k}} \cdot \hat{\mathbf{r}}) = \frac{4\pi}{2\ell + 1} \sum_{m=-\ell}^{\ell} Y_{\ell m}(\hat{\mathbf{k}}) \int d\mathbf{r} F(\mathbf{r}) Y_{\ell m}^*(\hat{\mathbf{r}}) e^{i\mathbf{k}\cdot\mathbf{r}}. \quad (16)$$

This is based on the Yamamoto estimator (Yamamoto et al. 2006), and makes use of the Addition Theorem to reduce the number of Fast Fourier Transforms (FFTs)¹ required in the calculation (Hand et al. 2017)². The cross power spectrum, measured from the eBOSS DR16 samples using Equation (15), is featured in Figure 4.

For the power spectrum analysis, one has to model the effect from the survey geometry carefully, as this window function effect can alter the power spectrum multipoles³, as formulated in Wilson et al. (2017). The survey window function can be measured from the randoms by a pair-counting approach (Wilson et al. 2017; Zhao et al. 2020; Gil-Marín et al. 2020), namely,

$$W_\ell^{\text{AB}}(s) = \frac{(2\ell + 1)}{I_{\text{AB}}\eta^{-2}} \sum_{i,j}^{N_{\text{ran}}} \frac{w_{\text{tot}}^{\text{A}}(\mathbf{x}_i) w_{\text{tot}}^{\text{B}}(\mathbf{x}_j + \mathbf{s})}{4\pi s^3 \Delta(\log s)} \mathcal{L}_\ell(\hat{\mathbf{x}}_{\text{los}} \cdot \hat{\mathbf{s}}), \quad (17)$$

where η is the ratio of the weighted numbers of the data and random cases. Note that the same normalization factor I_{AB} appears in both Equations (15) and (17), to guarantee that the measured and theoretical power spectra are normalized in the same way (de Mattia & Ruhlmann-Kleider 2019).

¹ The FFT library commonly used is available at <http://www.fftw.org/>

² The FFT-based estimator for the power spectrum multipoles was first developed in Bianchi et al. (2015); Scoccimarro (2015) applying a decomposition of $\mathcal{L}_\ell(\hat{\mathbf{k}} \cdot \hat{\mathbf{r}})$ in Cartesian coordinates, thus it requires a larger number of FFTs than the estimator expressed in Eqs. (15) and (16).

³ Note that the window function has no effect on the correlation function, because the effect changes the $DD(DR)$ and the RR pairs in the same, multiplicative way, thus it is perfectly canceled out in the Landy & Szalay estimator written in Eq. (11).

3.2 Modeling the Galaxy Clustering

This section describes the models commonly employed for a multi-tracer survey in both configuration space and Fourier space.

3.2.1 Modeling the 2-point correlation function

In configuration space, the Gaussian Streaming Model (GSM) (Reid & White 2011; Wang et al. 2014) is widely utilized for modeling the full-shape of the 2-point correlation function,

$$1 + \xi(s_\perp, s_\parallel) = \int \frac{dy}{\sqrt{2\pi [\sigma_{12}^2(r, \mu) + \sigma_{\text{FOG}}^2]}} [1 + \xi(r)] \times \exp \left\{ -\frac{[s_\parallel - y - \mu v_{12}(r)]^2}{2 [\sigma_{12}^2(r, \mu) + \sigma_{\text{FOG}}^2]} \right\}, \quad (18)$$

where $s_\parallel \equiv s\mu$ and $s_\perp \equiv s\sqrt{(1 - \mu^2)}$ represent the separation of pairs along and across the line of sight, respectively; $\xi(r)$ is the real-space correlation function as a function of the real-space separation r ; $v_{12}(r)$ is the mean infall velocity of galaxies separated by r ; and $\sigma_{12}(r, \mu)$ is the pairwise velocity dispersion of galaxies. The parameter σ_{FOG} is to account for the Fingers-of-God effect on nonlinear scales. Ingredients including $\xi(r)$, $v_{12}(r)$ and $\sigma_{12}(r, \mu)$ are evaluated considering the Convolution Lagrangian Perturbation Theory (CLPT)⁴ (Carlson et al. 2013; Wang et al. 2014), which requires a linear power spectrum, and two bias parameters $\langle F' \rangle$ and $\langle F'' \rangle$. The bias parameters can either be treated as

⁴ Publicly available at https://github.com/w11745881210/CLPT_GSRSD.

independent parameters in the fitting, or be related using the peak-background split argument (Matsubara 2008).

To generalize Equation (18) for the multi-tracer case, one only needs to perform the following transformation on the bias parameters, which appeared in the CLPT calculation (Carlson et al. 2013; Wang et al. 2014),

$$\begin{aligned}
\langle F' \rangle &\rightarrow \frac{1}{2} (\langle F'_A \rangle + \langle F'_B \rangle) \\
\langle F'' \rangle &\rightarrow \frac{1}{2} (\langle F''_A \rangle + \langle F''_B \rangle) \\
\langle F' \rangle^2 &\rightarrow \langle F'_A \rangle \langle F'_B \rangle \\
\langle F'' \rangle^2 &\rightarrow \langle F''_A \rangle \langle F''_B \rangle \\
\langle F' \rangle \langle F'' \rangle &\rightarrow \frac{1}{2} (\langle F'_A \rangle \langle F''_B \rangle + \langle F''_A \rangle \langle F'_B \rangle).
\end{aligned} \tag{19}$$

Finally, $\xi(s_\perp, s_\parallel)$ needs to be replaced with $\xi(s'_\perp, s'_\parallel)$ to account for the Alcock-Paczynski (AP) effect (Alcock & Paczynski 1979), which is an anisotropy in the clustering

if a wrong cosmology is applied to convert the redshifts into distances. The AP effect transforms the coordinates in the following way,

$$s'_\perp = \alpha_\perp s_\perp, \quad s'_\parallel = \alpha_\parallel s_\parallel, \tag{20}$$

with

$$\alpha_\perp = \frac{D_M(z)r_d^{\text{fid}}}{D_M^{\text{fid}}(z)r_d}, \quad \alpha_\parallel = \frac{D_H(z)r_d^{\text{fid}}}{D_H^{\text{fid}}(z)r_d}. \tag{21}$$

where r_d represents the sound horizon at recombination, $D_M(z) \equiv (1+z)D_A(z)$ and $D_A(z)$ is the angular diameter distance. $D_H(z) = c/H(z)$ and $H(z)$ is the Hubble expansion parameter. The superscript ‘fid’ denotes the corresponding values in a fiducial cosmology.

3.2.2 Modeling the power spectrum

In Fourier space, the TNS model (Taruya et al. 2010) is proven to be robust up to quasi-nonlinear scales, and thus has been widely employed by the BOSS and eBOSS collaborations for data analysis (Beutler et al. 2017; Gil-Marín et al. 2018; Zhao et al. 2019; Gil-Marín et al. 2020; de Mattia et al. 2020; Zhao et al. 2020). An extension of the TNS model for a multi-tracer survey was recently developed by Zhao et al. (2020),

$$P_g^{\text{AB}}(k, \mu) = D_{\text{FoG}}(k, \mu) [P_{g,\delta\delta}^{\text{AB}}(k) + 2f\mu^2 P_{g,\delta\theta}^{\text{AB}}(k) + f^2\mu^4 P_{\theta\theta}^{\text{AB}}(k) + A^{\text{AB}}(k, \mu) + B^{\text{AB}}(k, \mu)], \tag{22}$$

where

$$\begin{aligned}
P_{g,\delta\delta}^{\text{AB}}(k) &= b_1^A b_1^B P_{\delta\delta}(k) + (b_1^A b_2^B + b_1^B b_2^A) P_{b2,\delta}(k) + (b_{s2}^A b_1^B + b_{s2}^B b_1^A) P_{bs2,\delta}(k) \\
&\quad + (b_{s2}^A b_2^B + b_{s2}^B b_2^A) P_{b2s2}(k) + (b_{3nl}^A b_1^B + b_{3nl}^B b_1^A) \sigma_3^2(k) P_m^L(k) \\
&\quad + b_2^A b_2^B P_{b22}(k) + b_{s2}^A b_{s2}^B P_{bs22}(k) + N_{\text{AB}} \\
P_{g,\delta\theta}^{\text{AB}}(k) &= \frac{1}{2} [(b_1^A + b_1^B), P_{\delta\theta}(k) + (b_2^A + b_2^B) P_{b2,\theta}(k) + (b_{s2}^A + b_{s2}^B) P_{bs2,\theta}(k)], \\
&\quad + (b_{3nl}^A + b_{3nl}^B) \sigma_3^2(k) P_m^L(k)] \\
P_{g,\theta\theta}(k) &= P_{\theta\theta}(k), \\
D_{\text{FoG}}(k, \mu) &= \left\{ 1 + [k\mu\sigma_v]^2 / 2 \right\}^{-2}.
\end{aligned} \tag{23}$$

The subscripts δ and θ are the over-density and velocity divergence fields, respectively, and $P_{\delta\delta}$, $P_{\delta\theta}$ and $P_{\theta\theta}$ denote the quasi-nonlinear auto- or cross-power spectrum, evaluated utilizing tools such as regularized perturbation theory (RegPT) (Taruya et al. 2012). $P_m^L(k)$ signifies the linear power spectrum, and terms b_1 and b_2 stand for the linear bias and the second-order local bias, respectively. The second-order non-local bias b_{s2} and the third-order non-local bias b_{3nl} can be related to the linear bias via (Chan et al. 2012),

$$b_{s2} = -\frac{4}{7}(b_1 - 1), \quad b_{3nl} = \frac{32}{315}(b_1 - 1). \tag{24}$$

The correction terms A and B for a multi-tracer survey require a non-trivial extension, and we refer the readers to

Appendix A of Zhao et al. (2020) for a full derivation and result.⁵

⁵ A Fortran code for computing these correction terms is available at: http://www2.yukawa.kyoto-u.ac.jp/~atsushi.taruya/cpt_pack.html

As for the correlation functions, the AP effect distorts the power spectrum by changing (k, μ) to (k', μ') in the following way (Ballinger et al. 1996),

$$\begin{aligned} k' &= \frac{k}{\alpha_{\perp}} \left[1 + \mu^2 \left(\frac{1}{F^2} - 1 \right) \right]^{1/2}; \\ \mu' &= \frac{\mu}{F} \left[1 + \mu^2 \left(\frac{1}{F^2} - 1 \right) \right]^{-1/2}, \end{aligned} \quad (25)$$

where $F = \alpha_{\parallel}/\alpha_{\perp}$. The theoretical power spectrum multipoles are,

$$P_{\ell}^{\text{AB}}(k) = \frac{(2\ell + 1)}{2\alpha_{\perp}^2 \alpha_{\parallel}} \int_{-1}^1 d\mu P_{\text{g}}^{\text{AB}} [k'(k, \mu), \mu'(\mu)] \mathcal{L}_{\ell}(\mu), \quad (26)$$

where \mathcal{L}_{ℓ} is the Legendre polynomial of order ℓ .

As mentioned in Section 3.1.2, the measured power spectrum multipoles are the true ones convolved with the survey window function shown in Equation (17), therefore the same convolution needs to be applied to the theoretical prediction, for a fair comparison. An efficient way, which is based on the FFTLOG algorithm (Hamilton 2000)⁶, for evaluating this convolution is developed in Wilson et al. (2017).

3.3 Parameter Estimation

With measurements of the 2-point correlation function or power spectrum multipoles from a galaxy sample, the corresponding data covariance matrix measured from the mock catalogs (see Zhao et al. 2020 for an example of this procedure) and a theoretical template, one can perform a likelihood analysis to estimate parameters including $\alpha_{\parallel}, \alpha_{\perp}, f\sigma_8$, as well as f_{NL} applying efficient algorithms including Monte Carlo Markov Chain (MCMC), as implemented in the CosmoMC⁷ (Lewis & Bridle 2002) and Getdist⁸ (Lewis 2019) packages.

4 WORKED EXAMPLES

This section showcases a few worked examples of recent multi-tracer analyses, based on the GAMA, BOSS and eBOSS surveys.

4.1 A Multi-tracer Analysis for the GAMA Survey

The first multi-tracer analysis was performed on the GAMA survey (Blake et al. 2013). GAMA provided a

⁶ Publicly available at <https://jila.colorado.edu/~ajsh/FFTLog/>

⁷ Publicly available at <https://cosmologist.info/cosmomc/>

⁸ Publicly available at <https://github.com/cmbant/getdist>

sample of 178 579 galaxies within the redshift range of $0 < z < 0.5$ with a coverage area of 180 deg^2 . To meet the requirement for a multi-tracer analysis, the entire sample was split into two subsamples by color and luminosity. A joint constraint on f (the logarithmic growth rate) and σ_v (the FoG damping parameter) is demonstrated in Figure 5, where two subsamples, split by color (left panels) and luminosity (right panels), are used for a multi-tracer analysis in two redshift slices $0 < z < 0.25$ and $0.25 < z < 0.5$, respectively. It is found that the precision of f from the joint fits (black solid lines) can be improved by 10–20%, compared to that from one individual subsample (blue dashed lines for tracer-1 (tr-1) and the red dotted lines for tracer 2 (tr-2)).

4.2 A Multi-tracer Analysis for the BOSS Survey

Also splitting samples by color, Ross et al. (2014) performed a multi-tracer analysis on the ‘CMASS’ sample released in the SDSS-III BOSS DR10. This original CMASS DR10 sample consists of 540 505 galaxies within $0.43 < z < 0.7$. Based on a color-selection, ‘Red’ and ‘Blue’ subsamples are created with a relative bias being $b_{\text{Red}}/b_{\text{Blue}} = 1.39 \pm 0.04$. Note that the color-selected samples only have 254 936 galaxies in total, which halves the number of the original, unsplit sample.

The monopole and quadrupole of the color-selected samples and their cross-correlation are plotted in Figure 6, which yield a constraint on the RSD parameter (with relevant parameters marginalized over) (Ross et al. 2014),

$$\begin{aligned} f\sigma_{8,\text{Red}} &= 0.511 \pm 0.083; \\ f\sigma_{8,\text{Blue}} &= 0.509 \pm 0.085; \\ f\sigma_{8,\text{Cross}} &= 0.423 \pm 0.061. \end{aligned} \quad (27)$$

This clearly demonstrates the importance of the cross correlation function for constraining the RSD parameter: it provides a better constraint on $f\sigma_8$ on its own, namely, the uncertainty on $f\sigma_8$ is reduced by $\sim 25\%$ using the cross-correlation function, compared to that using the auto-correlation function. Combining the auto- and cross-correlation further improves the constraint to $f\sigma_{8,\text{comb}} = 0.443 \pm 0.055$, which is comparable to that using the original, unsplit sample with double the number of galaxies, $f\sigma_{8,\text{full}} = 0.422 \pm 0.051$.

4.3 A Multi-tracer Analysis for the eBOSS Survey

As mentioned in Section 1, the SDSS-IV/eBOSS delivered observations of multiple tracers within one galaxy survey. eBOSS observes three types of discrete tracers, the LRGs, ELGs and quasars (Dawson et al. 2016). The LRGs and ELGs significantly overlap, namely, the overlapping sky

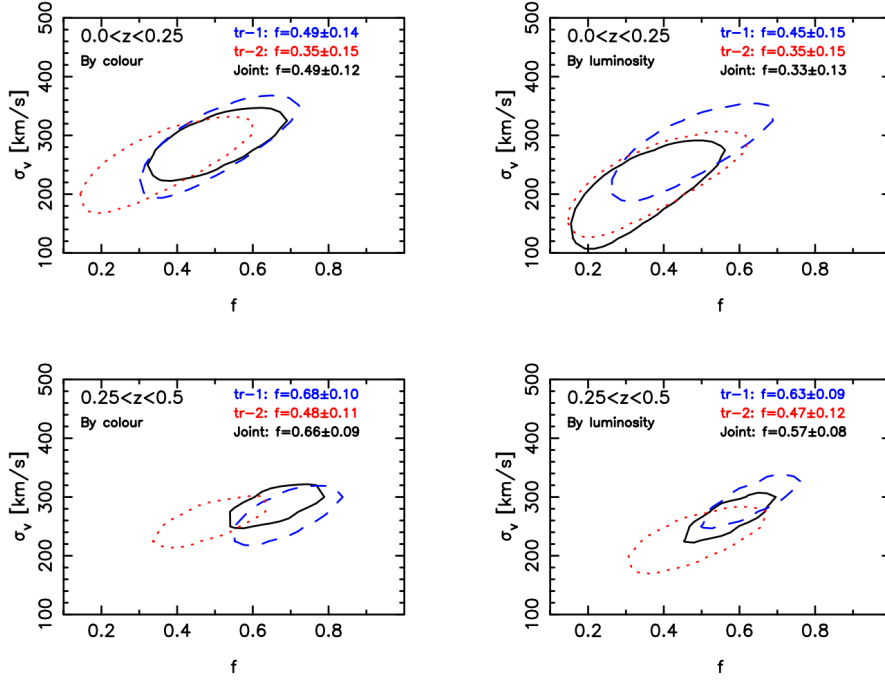


Fig. 5 The joint constraint on f and σ_v presented in [Blake et al. \(2013\)](#). The GAMA sample is split into two using color (*left panels*) and luminosity (*right*), respectively. The *blue dashed*, *red dotted* and *black solid contours* signify constraints using tracer 1 (tr-1), tracer 2 (tr-2) and the combined (Joint), respectively. The analysis is performed on galaxies in two redshift slices: $0 < z < 0.25$ (*upper*) and $0.25 < z < 0.5$ (*lower*).

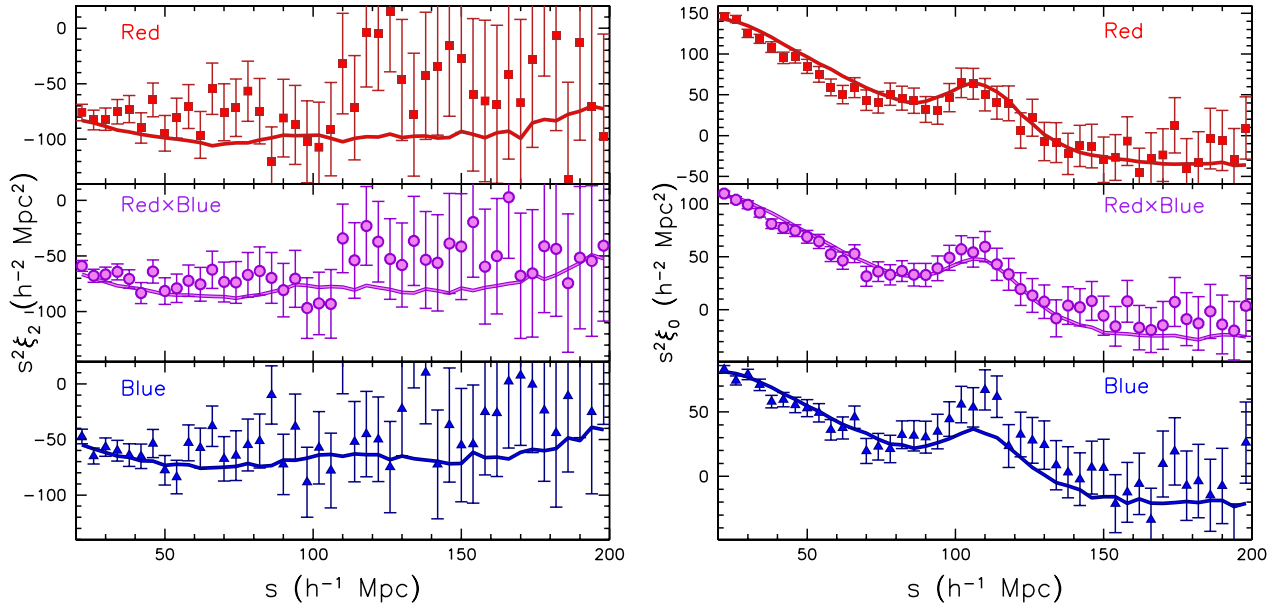


Fig. 6 The correlation function monopole (*left*) and quadrupole (*right*), measured from the BOSS DR10 color-split samples. The top and bottom panels are for the ‘Red’ and ‘Blue’ samples, respectively, while the middle panels feature the measurement from the cross-correlation. Figure adopted from [Ross et al. \(2014\)](#).

coverage is 730 deg^2 within the redshift range of $0.6 < z < 1.0$. Moreover, the LRGs and ELGs have a relative linear bias around 1.5 ([Zhao et al. 2020](#)), making the

eBOSS LRGs and ELGs ideal samples for a multi-tracer analysis.

A cross-correlation signal is detected well between the eBOSS LRGs and ELGs in both configuration ([Wang](#)

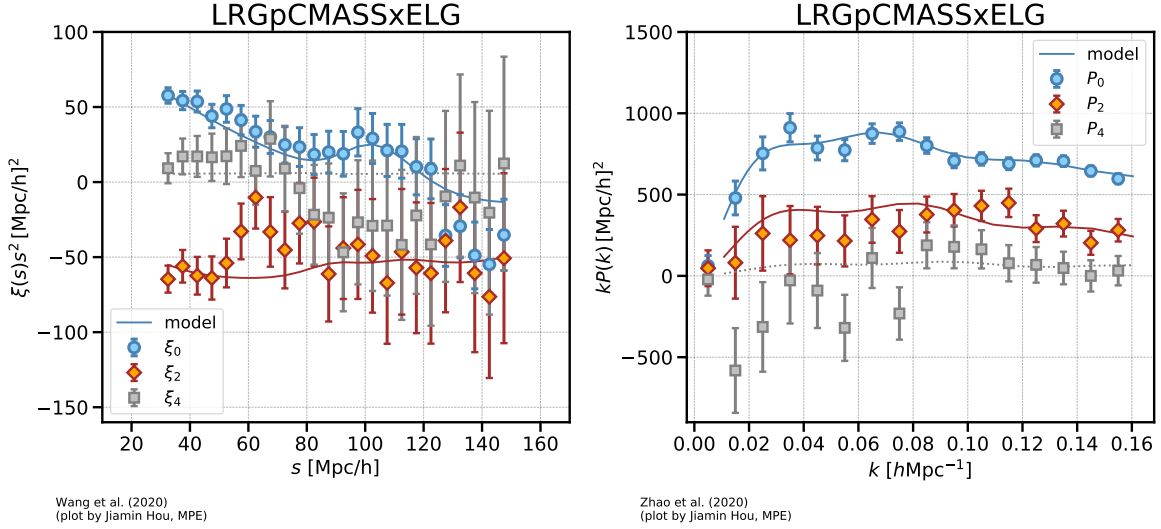


Fig. 7 *Left*: The cross-correlation function multipoles measured from the eBOSS DR16 LRG and ELG samples (data points with error bars), with the best-fit model over-plotted in solid curves (Wang et al. 2020); *Right*: the corresponding quantities in Fourier space, as analyzed in Zhao et al. (2020). The plots are made by Jiamin Hou (MPE), and are available at <https://www.sdss.org/science/final-bao-and-rsd-measurements/>.

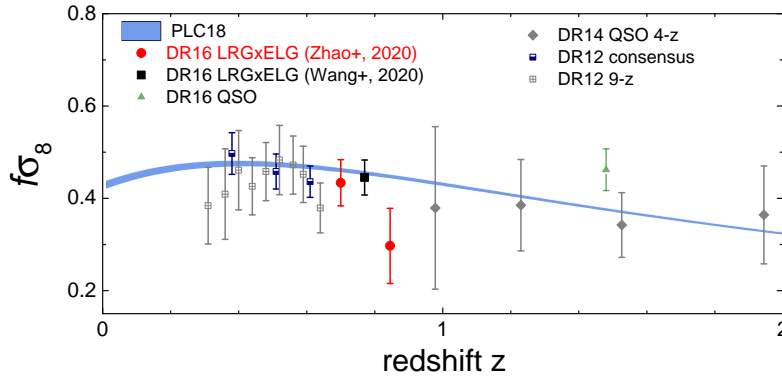


Fig. 8 A compilation of $f\sigma_8$ measurements from the SDSS BOSS and eBOSS surveys, including those from the latest multi-tracer analysis of the eBOSS DR16 sample in configuration space (DR16 LRG \times ELG) (Wang et al. 2020) and Fourier-space (DR16 LRG \times ELG) (Zhao et al. 2020), the consensus result from eBOSS DR16 QSOs (DR16 QSO) (Hou et al. 2020), the tomographic RSD measurement from the eBOSS DR14 QSO sample applying the optimal redshift weighting method (DR14 QSO 4-z) (Zhao et al. 2019) and the tomographic RSD measurement from the BOSS DR12 sample in Fourier space (DR12 9-z) (Zheng et al. 2019). For reference, the blue band is the 68% CL constraint derived from Planck 2018 observations in a Λ CDM cosmology (Planck Collaboration et al. 2018).

et al. 2020) and Fourier space (Zhao et al. 2020), as displayed in Figure 7 (data points with error bars) together with theory curves of the best-fit model (solid lines). The cross-correlation can not only reduce the statistical error of the RSD parameters, it also helps with mitigating the systematic errors, because the contamination in the photometry of each tracer, which is one possible source of observational systematics, does not correlate with each other. Take the eBOSS ELG sample for example, it is known to be affected by photometric systematics, thus the correlation function and power spectrum of the ELG sample have to be specifically processed for a

cosmological analysis (Tamone et al. 2020; de Mattia et al. 2020). However, the cross correlation function and cross power spectrum are largely immune to this type of systematics, as demonstrated utilizing the mock catalogs from Wang et al. (2020); Zhao et al. (2020).

Figure 8 depicts the measurement of $f\sigma_8$ from the eBOSS multi-tracer analyses, with other recent measurements from BOSS and eBOSS programs. Note that the effective redshifts of the LRG and ELG samples are different, and Zhao et al. (2020) and Wang et al. (2020) take different approaches to account for this effect (both approaches are validated by the mock tests), thus the

resultant measurements are at different effective redshifts, *e.g.*, Zhao et al. (2020) report two measurements at $z = 0.70$ and 0.845 , respectively, while Wang et al. (2020) only measure at $z = 0.77$. While a direct comparison is not straightforward at this level, Zhao et al. (2020) performed an additional measurement at $z = 0.77$, and found a consistency with Wang et al. (2020). In this analysis, it is found that the constraint on $f\sigma_8$ gets improved by approximately 12%, compared to that using the LRGs alone (Wang et al. 2020).

5 CONCLUSION AND DISCUSSIONS

Stepping into the stage-IV era of galaxy surveys, we are seeking statistical and theoretical methods to improve the precision on the measured cosmological parameters, which is limited by the cosmic variance and shot noise. One promising way to beat the cosmic variance is to contrast the 2-point statistics of different tracers, yielding a quantity of cosmological importance, which is free from the cosmic variance.

In this brief review, we present the basic idea of the multi-tracer method, outline a procedure for performing multi-tracer analysis, followed by a few worked examples based on large galaxy surveys, which have clearly demonstrated the efficacy of this method.

The newly-started Dark Energy Spectroscopic Instrument (DESI; DESI Collaboration et al. 2016 a,b) is a typical multi-tracer survey, whose LRG and ELG targets do overlap significantly across a wide redshift range with a much higher number density than that of eBOSS. This makes it ideal for a multi-tracer analysis for improving the statistical precision of the RSD and primordial non-Gaussianity. The multi-tracer analysis also helps with the observational systematics through cross-correlation between tracers, in addition to mitigating the systematics by a better modeling and pipeline for processing the raw observations.

Acknowledgements GBZ is supported by the National Key Basic Research and Development Program of China (No. 2018YFA0404503), and a grant from the CAS Interdisciplinary Innovation Team. YW is supported by the Nebula Talents Program of NAOC. YW and GBZ are supported by the National Natural Science Foundation of China (Grant Nos. 11925303, 11720101004, 11673025 and 11890691).

Funding for the Sloan Digital Sky Survey IV has been provided by the Alfred P. Sloan Foundation, the U.S. Department of Energy Office of Science, and the Participating Institutions. SDSS-IV acknowledges support and resources from the Center for High-Performance

Computing at the University of Utah. The SDSS web site is <http://www.sdss.org/>.

SDSS-IV is managed by the Astrophysical Research Consortium for the Participating Institutions of the SDSS Collaboration including the Brazilian Participation Group, the Carnegie Institution for Science, Carnegie Mellon University, the Chilean Participation Group, the French Participation Group, Harvard-Smithsonian Center for Astrophysics, Instituto de Astrofísica de Canarias, The Johns Hopkins University, Kavli Institute for the Physics and Mathematics of the Universe (IPMU) / University of Tokyo, the Korean Participation Group, Lawrence Berkeley National Laboratory, Leibniz Institut für Astrophysik Potsdam (AIP), Max-Planck-Institut für Astronomie (MPIA Heidelberg), Max-Planck-Institut für Astrophysik (MPA Garching), Max-Planck-Institut für Extraterrestrische Physik (MPE), National Astronomical Observatories of China, New Mexico State University, New York University, University of Notre Dame, Observatório Nacional / MCTI, The Ohio State University, Pennsylvania State University, Shanghai Astronomical Observatory, United Kingdom Participation Group, Universidad Nacional Autónoma de México, University of Arizona, University of Colorado Boulder, University of Oxford, University of Portsmouth, University of Utah, University of Virginia, University of Washington, University of Wisconsin, Vanderbilt University, and Yale University.

References

- Abramo, L. R. 2012, MNRAS, 420, 2042
- Abramo, L. R. & Amendola, L. 2019, J. Cosmol. Astropart. Phys., 2019, 030
- Abramo, L. R. & Leonard, K. E. 2013, MNRAS, 432, 318
- Abramo, L. R., Secco, L. F., & Loureiro, A. 2016, MNRAS, 455, 3871
- Abazajian, K. N., Adelman-McCarthy, J. K., Agüeros, M. A., et al. 2009, ApJS, 182, 543
- Alam, S., Ata, M., Bailey, S., et al. 2017, MNRAS, 470, 2617
- Alarcon, A., Eriksen, M., & Gaztanaga, E. 2018, MNRAS, 473, 1444
- Alcock, C. & Paczynski, B. 1979, Nature, 281, 358
- Anderson, L., Aubourg, E., Bailey, S., et al. 2012, MNRAS, 427, 3435
- Baldry, I. K., Robotham, A. S. G., Hill, D. T., et al. 2010, MNRAS, 404, 86
- Ballinger, W. E., Peacock, J. A., & Heavens, A. F. 1996, MNRAS, 282, 877
- Bennett, C. L., Halpern, M., Hinshaw, G., et al. 2003, ApJS, 148, 1
- Bernstein, G. M., & Cai, Y.-C. 2011, MNRAS, 416, 3009
- Betoule, M., Kessler, R., Guy, J., et al. 2014, A&A, 568, A22

- Beutler, F., Blake, C., Colless, M., et al. 2011, *MNRAS*, 416, 3017
- Beutler, F., Blake, C., Koda, J., et al. 2016, *MNRAS*, 455, 3230
- Beutler, F., Seo, H.-J., Saito, S., et al. 2017, *MNRAS*, 466, 2242
- Blake, C., Brough, S., Couch, W., et al. 2008, *Astronomy and Geophysics*, 49, 5.19
- Blake, C., Kazin, E. A., Beutler, F., et al. 2011, *MNRAS*, 418, 1707
- Blake, C., Baldry, I. K., Bland-Hawthorn, J., et al. 2013, *MNRAS*, 436, 3089
- Bianchi, D., Gil-Marín, H., Ruggeri, R., et al. 2015, *MNRAS*, 453, L11
- Boschetti, R., Abramo, L. R., & Amendola, L. 2020, arXiv:2005.02465
- Cai, Y.-C. & Bernstein, G. 2012, *MNRAS*, 422, 1045
- Carlson, J., Reid, B., & White, M. 2013, *MNRAS*, 429, 1674
- Chan, K. C., Scoccimarro, R., & Sheth, R. K. 2012, *Phys. Rev. D*, 85, 083509
- Cole, S., Percival, W. J., Peacock, J. A., et al. 2005, *MNRAS*, 362, 505
- Colless, M., Dalton, G., Maddox, S., et al. 2001, *MNRAS*, 328, 1039
- Dalal, N., Doré, O., Huterer, D., et al. 2008, *Phys. Rev. D*, 77, 123514
- D’Andrea, C. B., Smith, M., Sullivan, M., et al. 2018, arXiv:1811.09565
- Davis, M. & Peebles, P. J. E. 1983, *ApJ*, 267, 465
- Dawson, K. S., Kneib, J.-P., Percival, W. J., et al. 2016, *AJ*, 151, 44
- de Mattia, A., & Ruhlmann-Kleider, V. 2019, *J. Cosmol. Astropart. Phys.*, 2019, 036
- de Mattia, A., Ruhlmann-Kleider, V., Raichoor, A., et al. 2020, arXiv:2007.09008
- DESI Collaboration, Aghamousa, A., Aguilar, J., et al. 2016, arXiv:1611.00036
- DESI Collaboration, Aghamousa, A., Aguilar, J., et al. 2016, arXiv:1611.00037
- Eisenstein, D. J., Zehavi, I., Hogg, D. W., et al. 2005, *ApJ*, 633, 560
- Eisenstein, D. J., Weinberg, D. H., Agol, E., et al. 2011, *AJ*, 142, 72
- Feldman, H. A., Kaiser, N., & Peacock, J. A. 1994, *ApJ*, 426, 23
- Ferramacho, L. D., Santos, M. G., Jarvis, M. J., et al. 2014, *MNRAS*, 442, 2511
- Fonseca, J., Camera, S., Santos, M. G., et al. 2015, *ApJL*, 812, L22
- Gil-Marín, H., Bautista, J. E., Paviot, R., et al. 2020, arXiv:2007.08994
- Gil-Marín, H., Guy, J., Zarrouk, P., et al. 2018, *MNRAS*, 477, 1604
- Gil-Marín, H., Wagner, C., Verde, L., et al. 2010, *MNRAS*, 407, 772
- Gomes, Z., Camera, S., Jarvis, M. J., et al. 2020, *MNRAS*, 492, 1513
- Gunn, J. E., Siegmund, W. A., Mannery, E. J., et al. 2006, *AJ*, 131, 2332
- Hamaus, N., Seljak, U., & Desjacques, V. 2011, *Phys. Rev. D*, 84, 083509
- Hamilton, A. J. S. 2000, *MNRAS*, 312, 257
- Hand, N., Li, Y., Slepian, Z., et al. 2017, *J. Cosmol. Astropart. Phys.*, 2017, 002
- Hinshaw, G., Larson, D., Komatsu, E., et al. 2013, *ApJS*, 208, 19
- Hou, J., Sánchez, A. G., Ross, A. J., et al. 2020, arXiv:2007.08998
- Huchra, J., Davis, M., & Latham, D. 1983, Cambridge: Smithsonian Center for Astrophysics
- Huterer, D. & Shafer, D. L. 2018, *Reports on Progress in Physics*, 81, 016901
- Jones, D. H., Read, M. A., Saunders, W., et al. 2009, *MNRAS*, 399, 683
- Kaiser, N. 1987, *MNRAS*, 227, 1
- Karagiannis, D., Shanks, T., & Ross, N. P. 2014, *MNRAS*, 441, 486
- Koyama, K. 2016, *Reports on Progress in Physics*, 79, 046902
- Landy, S. D. & Szalay, A. S. 1993, *ApJ*, 412, 64
- Lewis, A. 2019, arXiv:1910.13970
- Lewis, A. & Bridle, S. 2002, *Phys. Rev. D*, 66, 103511
- LSST Science Collaboration, Abell, P. A., Allison, J., et al. 2009, arXiv:0912.0201
- Marín, F. A., Beutler, F., Blake, C., et al. 2016, *MNRAS*, 455, 4046
- Matsubara, T. 2008, *Phys. Rev. D*, 78, 083519
- McDonald, P. & Seljak, U. 2009, *J. Cosmol. Astropart. Phys.*, 2009, 007
- Mueller, E.-M., Percival, W. J., & Ruggeri, R. 2019, *MNRAS*, 485, 4160
- Nikoloudakis, N., Shanks, T., & Sawangwit, U. 2013, *MNRAS*, 429, 2032
- Padmanabhan, N., Xu, X., Eisenstein, D. J., et al. 2012, *MNRAS*, 427, 2132
- Peacock, J. A. & Dodds, S. J. 1994, *MNRAS*, 267, 1020
- Peacock, J. A., Cole, S., Norberg, P., et al. 2001, *Nature*, 410, 169
- Reid, B. A. & White, M. 2011, *MNRAS*, 417, 1913
- Percival, W. J., Baugh, C. M., Bland-Hawthorn, J., et al. 2001, *MNRAS*, 327, 1297
- Percival, W. J., Cole, S., Eisenstein, D. J., et al. 2007, *MNRAS*, 381, 1053
- Perlmutter, S., Aldering, G., Goldhaber, G., et al. 1999, *ApJ*, 517, 565
- Planck Collaboration, Aghanim, N., Akrami, Y., et al. 2018, arXiv:1807.06209
- Riess, A. G., Filippenko, A. V., Challis, P., et al. 1998, *AJ*, 116, 1009

- Riess, A. G., Strolger, L.-G., Casertano, S., et al. 2007, *ApJ*, 659, 98
- Ross, A. J., Percival, W. J., Carnero, A., et al. 2013, *MNRAS*, 428, 1116
- Ross, A. J., Samushia, L., Burden, A., et al. 2014, *MNRAS*, 437, 1109
- Ross, A. J., Samushia, L., Howlett, C., et al. 2015, *MNRAS*, 449, 835
- Scoccimarro, R. 2004, *Phys. Rev. D*, 70, 083007
- Scoccimarro, R. 2015, *Phys. Rev. D*, 92, 083532
- Scolnic, D. M., Jones, D. O., Rest, A., et al. 2018, *ApJ*, 859, 101
- Seljak, U. 2009, *Phys. Rev. Lett.*, 102, 021302
- Shectman, S. A., Landy, S. D., Oemler, A., et al. 1996, *ApJ*, 470, 172
- Slosar, A., Hirata, C., Seljak, U., et al. 2008, *J. Cosmol. Astropart. Phys.*, 2008, 031
- Sullivan, M., Guy, J., Conley, A., et al. 2011, *ApJ*, 737, 102
- Suzuki, N., Rubin, D., Lidman, C., et al. 2012, *ApJ*, 746, 85
- Tamone, A., Raichoor, A., Zhao, C., et al. 2020, *arXiv:2007.09009*
- Tanidis, K., & Camera, S. 2020, *arXiv:2009.05584*
- Taruya, A., Bernardeau, F., Nishimichi, T., et al. 2012, *Phys. Rev. D*, 86, 103528
- Taruya, A., Nishimichi, T., & Saito, S. 2010, *Phys. Rev. D*, 82, 063522
- Tegmark, M., Taylor, A. N., & Heavens, A. F. 1997, *ApJ*, 480, 22
- Viljoen, J.-A., Fonseca, J., & Maartens, R. 2020, *arXiv:2007.04656*
- Wands, D. 2010, *Classical and Quantum Gravity*, 27, 124002
- Wang, J. X., & Ip, W.-H. 2020, *RAA (Research in Astronomy and Astrophysics)*, 20, 157
- Wang, L., Reid, B., & White, M. 2014, *MNRAS*, 437, 588
- Wang, Y., Zhao, G.-B., Zhao, C., et al. 2020, *MNRAS*, doi:10.1093/mnras/staa2593
- White, M., Song, Y.-S., & Percival, W. J. 2009, *MNRAS*, 397, 1348
- Wilson, M. J., Peacock, J. A., Taylor, A. N., et al. 2017, *MNRAS*, 464, 3121
- Yamamoto, K., Nakamichi, M., Kamino, A., et al. 2006, *PASJ*, 58, 93
- Yamauchi, D., Takahashi, K., & Oguri, M. 2014, *Phys. Rev. D*, 90, 083520
- York, D. G., Adelman, J., Anderson, J. E., et al. 2000, *AJ*, 120, 1579
- Zhao, C., Chuang, C.-H., Bautista, J., et al. 2020, *arXiv:2007.08997*
- Zhao, G.-B., Wang, Y., Ross, A. J., et al. 2016, *MNRAS*, 457, 2377
- Zhao, G.-B., Wang, Y., Saito, S., et al. 2019, *MNRAS*, 482, 3497
- Zhao, G.-B., Wang, Y., Taruya, A., et al. 2020, *arXiv:2007.09011*
- Zheng, J., Zhao, G.-B., Li, J., et al. 2019, *MNRAS*, 484, 442